frontiers | Frontiers in Materials

TYPE Original Research
PUBLISHED 01 March 2023
DOI 10.3389/fmats.2023.1131412

OPEN ACCESS

EDITED BY
Santosh Kumar,
Liaocheng University, China

REVIEWED BY
Dharmendra Kumar,
Madan Mohan Malaviya University of Technology, India
Purnendu Shekhar Pandey,
GL Bajaj Institute of Technology and Management (GLBITM), India

*CORRESPONDENCE
Shatrughna Kumar,
shatruism15@gmail.com

SPECIALTY SECTION
This article was submitted to Semiconducting Materials and Devices, a section of the journal Frontiers in Materials

RECEIVED 16 January 2023
ACCEPTED 06 February 2023
PUBLISHED 01 March 2023

CITATION
Kumar S, Yadav A and Malomed BA (2023), High performance surface plasmon resonance based sensor using black phosphorus and magnesium oxide adhesion layer.
Front. Mater. 10:1131412.
doi: 10.3389/fmats.2023.1131412

High performance surface plasmon resonance based sensor using black phosphorus and magnesium oxide adhesion layer

Shatrughna Kumar[1,2]*, Archana Yadav[3,4] and Boris A. Malomed[2,5]

[1]Department of Electronics Engineering, Indian Institute of Technology (Indian Institute of Mines), Dhanbad, Jharkhand, India, [2]Department of Physical Electronics, School of Electrical Engineering, Faculty of Engineering and Center for Light-Matter Interaction, Tel Aviv University, Tel Aviv, Israel, [3]Department of Electronics and Communication Engineering, ASET Amity University, Nodia, Uttar Pradesh, India, [4]Department of Electronics and Communication Engineering, Faculty of Engineering Integral University, Lucknow, Uttar Pradesh, India, [5]Instituto de Alta Investigación, Universidad de Tarapacá, Arica, Chile

A five-layered Kretschmann configuration-based novel structure is designed for a highly sensitive surface plasmon resonance (SPR) sensor. An adhesion layer of magnesium oxide (MgO) is employed on the BK7 prism to avoid the adverse effects of metallic layers, which cause SPR broadening and a decrease in the resonance magnitude. A few layers of black phosphorus (BP) on top of the silver (Ag) metal layer are added to complete the structure, which becomes the BK7/MgO/Ag/BP configuration. The investigation is carried out using attenuated total reflection (ATR), while the widely used transfer matrix method (TMM) is applied to evaluate the performance of the SPR sensor. A separate analysis is performed using three thicknesses, 5 nm, 10 nm, and 15 nm of MgO, an optimized thickness of 40 nm of Ag, and eight layers of BP. The results revealed that the configuration BK7/MgO (10 nm)/Ag (40 nm)/BP (8 layers) delivers a maximum sensitivity (S) of 234°RIU^{-1}. Moreover, the configuration BK7/MgO (5 nm)/Ag (40 nm)/BP (8 layers) delivers a maximum figure of merit (FOM) of 38.18°RIU^{-1}. With these kinds of extraordinary features, it is expected that the proposed SPR sensor can be applied in different fields of biosensing.

KEYWORDS

surface plasmon resonance, sensitivity, black phosphorus, magnesium oxide, biosensor

1 Introduction

In the last two decades, surface plasmon resonance (SPR) technology has attracted massive attention from optical technologists because of its capability to solve a wide range of real-time unsolved challenges, specifically in the biomedical field. In the recent past, SPR-based sensing technology has been found to have tremendous development for detecting cancer cells, antibody characterization, glucose label detection, DNA hybridization, etc. SPR-based biosensors also find excellent applications for detecting and characterizing biomolecules, biochemicals, food, the environment, etc. (Nguyen et al., 2015; Bellassai et al., 2019; Asif et al., 2020; Mauriz, 2020; Taha et al., 2020). SPR sensing is based on attenuated total reflection (ATR), in which a sharp dip of the plasmonic resonance curve is obtained from the absorption of the incident light in the sensing medium (Akowuah et al., 2009; Verma et al., 2015; Li et al., 2017). More explicitly, the SPR sensing process changes the property of incident light after interacting with the analyte or sensing medium, as recorded in

the output light. The change in the input light could be in its frequency, amplitude, phase, or polarization as measured at the output. The SPR technique often uses a prism for coupling the incident light, and the variation in the incident angle of light interrogates the light. The change in the resonance angle (light angle) significantly depends on the analyte or sensing medium's refractive index (RI). An excellent-performing SPR sensor should be capable of measuring any minute change in the RI of the analyte. The SPR sensor's performance parameter, sensitivity (S), calculates the minute change in RI. Other key performance parameters are full width at half maximum (FWHM), detection accuracy (DA), and figure of merit (FOM), which can measure the quality of the SPR-based sensors (Verma et al., 2015).

Gold (Au) and silver (Ag) are the most commonly used plasmonic metals in the SPR phenomenon. Both materials have valuable features, such as high oxidation resistance due to aging, better absorption capacity, a lower complex RI that reduces the damping, and lower d-electron energy conduction, which is sufficient for SPR generation in the visible region (Rhodes et al., 2006; Rhodes et al., 2008; Khamh et al., 2018). However, the characteristic of both metals is like noble metals; there is a requirement for an adhesion layer to ensure firm bonding between the metal and the substrate layers. In the general technique to resolve the adhesion problem, metal layers like chromium (Cr), titanium (Ti), and tantalum (Ta) may be employed. However, incorporating the metal mentioned above adversely affects the plasmonic resonance phenomenon of metallic nanostructures. As a result, a high loss is measured, causing a significant damping effect. Hence, a broadening of the resonance curve and a decrease in its magnitude are recorded. As a result, the performance of the SPR decreases (Ekgasit et al., 2005; Jeppesen et al., 2010; Najiminaini et al., 2011; Otte et al., 2011; Hughes et al., 2012; Abbott et al., 2019). Some studies have proposed using oxides such as ITO, TiO_2, and Cr_2O_3 as adhesion layers to reduce losses (Aouani et al., 2009; Djaker et al., 2010; Sadri-Moshkenani et al., 2020). These oxides are low-loss materials at optical wavelengths. In a recent work (Sadri-Moshkenani et al., 2020), it has been demonstrated that low-loss magnesium oxide (MgO) could be the best alternative for the conventional adhesion layers and other adhesion layers proposed in the earlier works. Hence, in this work, MgO is chosen as the adhesive layer of the proposed structure of the SPR sensor.

On the other hand, recently, it has been observed that 2D materials are extensively utilized in the SPR-based sensors due to their extraordinary optical and electrical properties. Additionally, it possesses excellent thermal conductivity, mechanical conductivity, optical transparency, a high surface area-to-volume ratio, and large elasticity. These exceptional properties make them a suitable material for enhancing the performance of SPR-based sensors. Unlike other 2D materials, the BP consists of unique features like a single layer with a honeycomb lattice and is a direct bandgap semiconductor material. The energy bandgap of the BP can be tuned from 0.3 eV to 2 eV for bulk and single layer depending on the applied strain (Castellanos-Gomez, 2015). This feature of BP allows us to tailor its optical properties, which are responsible for SPR-based sensing applications. Moreover, compared to other 2D materials, BP exhibits a high absorption and adsorption coefficient, making it suitable for high sensitivity (Cho et al., 2016). Some other important SPR-based work using different techniques for various kinds of applications has been recently reported (Pandey and Raghuwanshi, 2022; Sahu et al., 2022).

With this motivation, the work proposes a Kretschmann configuration-based, novel five-layered structure for SPR refractive index sensor for various applications in biosensing. The first and last layers belong to the prism and sensing medium or analyte, respectively. An adhesion layer of MgO is placed between the prism and the silver metal layer. So, MgO and Ag correspond to the second and third layers, respectively. After that, a few layers of BP are incorporated into the Ag as the fourth layer of the structure. The next section of the work provides a detailed description of the proposed design of the SPR sensor. After that, in Section 3, mathematical modeling is presented for the calculation of reflectance and sensing parameters. The analysis of the result is presented in Section 4. Finally, a summary of the whole work is provided in the conclusion of Section 5.

2 Modelling of SPR sensor

One of the most widely used and accepted techniques to couple the light for the excitation of surface plasmon waves (SPWs) in SPR-based sensors is prism coupling. Several kinds of the prism may be employed to focus and couple the light that generally comes through the polarizer, as shown in Figure 1. However, if the light wave is launched directly at the metal surface, SPWs are still generated at the metal-dielectric interface, but the resonance condition is not satisfied due to insufficient light accumulation on the metal surface. Therefore, the requirement of the maximum accumulation of light on the metal surface can be fulfilled using the prism. The idea of prism coupling was first proposed by Otto (1968) and Zeng et al. (2013), which is called the Otto configuration. In this configuration, metal is placed above the prism, i.e., an air gap is maintained between the prism and metal layer. However, the evanescent wave that is generated at the interface of air and metal decreases exponentially from air to metal. Hence, it becomes difficult to maintain the air gap between the prism and the metal. The difficulty of the Otto configuration has been removed using a new configuration called the Kretschmann configuration, which is proposed by Otto, 1968. In the Kretschmann configuration, metal is deposited on the prism, i.e., no air gap is present between the metal and prism. It has been observed that the Kretschmann configuration is a more suitable configuration to improve the sensitivity of the SPR sensor as the associated technique decreases electromagnetic waves exponentially in both metal and dielectric media. Further, the dielectric layer is connected to a sensing medium in which biosamples are to be detected. Both of the configurations are based on the concept of attenuated total reflection (ATR). The present work focused on a Kretschmann configuration-based SPR sensor for biosensing, as shown in Figure 1.

Several kinds of the prism have different refractive indices, namely, CaF2, BK7, BAF10, BAK1, SF5, SF10, SF11, etc., available for light coupling. However, the work uses a BK7 glass prism due to its high efficiency and low refractive index (RI). BK7 makes it a good fit for pairing monochromatic, plane-polarized light generated at a wavelength of 633 nm by a He-Ne laser (Rahman et al., 2017). Therefore, the BK7 prism is considered the first layer of the structure of the proposed sensor. Thereafter, an adhesion layer of MgO is deposited on the BK7 prism, and this becomes the second layer of the system. Further, the silver (Ag) material is considered the

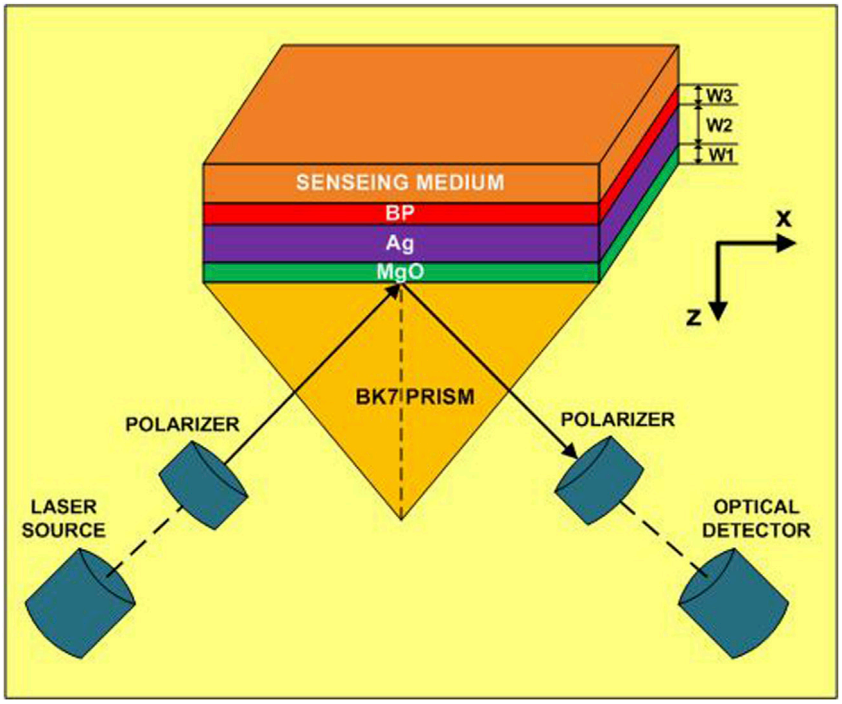

FIGURE 1
A five layered proposed structure for SPR biosensor based on Kretschmann configuration. The thickness of the layers of MgO, Ag, and BP are denoted by W1, W2, and W3 respectively.

TABLE 1 Thickness and refractive index of various materials of the proposed sensor at wavelength 633 nm.

Layer structure	Material used	Thickness (nm)	RI at 633 nm	References
Layer-01	BK7 glass prism	----	1.5151	Calculated
Layer-02	MnO	5/10/15	1.7346	Stephens and Malitson (1952)
Layer-02	Silver (Ag)	40	0.2184 + 3.5113*i	Calculated
Layer-04	BP	8*0.53	3.5 + 0.01*i	Zeng et al. (2015)
Layer-05	Sensing medium	----	1.335 + Δn	This work

plasmonic material for the proposed SPR sensor due to its superior character and excellent sensing performance. Additionally, selecting Ag over the most popular plasmonic material, gold (Au), makes the sensor cost-effective. Hence, the third layer of Ag metal is placed on the MgO. Now, a few layers of BP on top of the Ag are considered the fourth layer. Last, on top of the BP analyte or sensing medium is placed as the fifth and final layer of the sensor.

The operating wavelength of the incident light is considered to be 633 nm, to avoid the possibility of the enhancement of optical non-linearity and the Kerr effect at higher frequencies (Bruna and Borini, 2009; Sharma et al., 2010). Therefore, each material's RI and other parameters for the SPR sensor are taken cross-ponding to the operating wavelength of 633 nm. The RI of the BK7 glass prism for a given incident light wavelength ($\boldsymbol{\lambda}$) can now be calculated using Eq. 1, as reported in (Gupta and Sharma, 2005).

$$n_{BK7} = \left(1 + \frac{1.03961212\lambda^2}{\lambda^2 - 0.00600069867} + \frac{1.01046945\lambda^2}{\lambda^2 - 103.560653} + \frac{0.231792344\lambda^2}{\lambda^2 - 0.0200179144}\right)^{1/2} \quad (1)$$

On the other hand, the complex RI of the Ag for the given wavelength ($\boldsymbol{\lambda}$), which has been used here as a plasmonic material in the second layer of the proposed SPR sensor can be calculated using Eq. 2 following the Drude–Lorentz model (Rahman et al., 2020)

$$n_{Ag} = \left(1 - \frac{\lambda^2\lambda_c}{\lambda_p^2\,(\lambda_c + i\lambda)}\right)^{1/2} \quad (2)$$

Where, $\boldsymbol{\lambda}_p$, and $\boldsymbol{\lambda}_c$ denotes the plasmon wavelength and collision wavelength for Ag. The numerical values of the, $\boldsymbol{\lambda}_p$, and $\boldsymbol{\lambda}_c$ are consider as $1.4541 \times 10^{-7}m$ and $1.7614 \times 10^{-5}m$ respectively. All the RI od the considered material for the proposed sensors is summarised in Table 1.

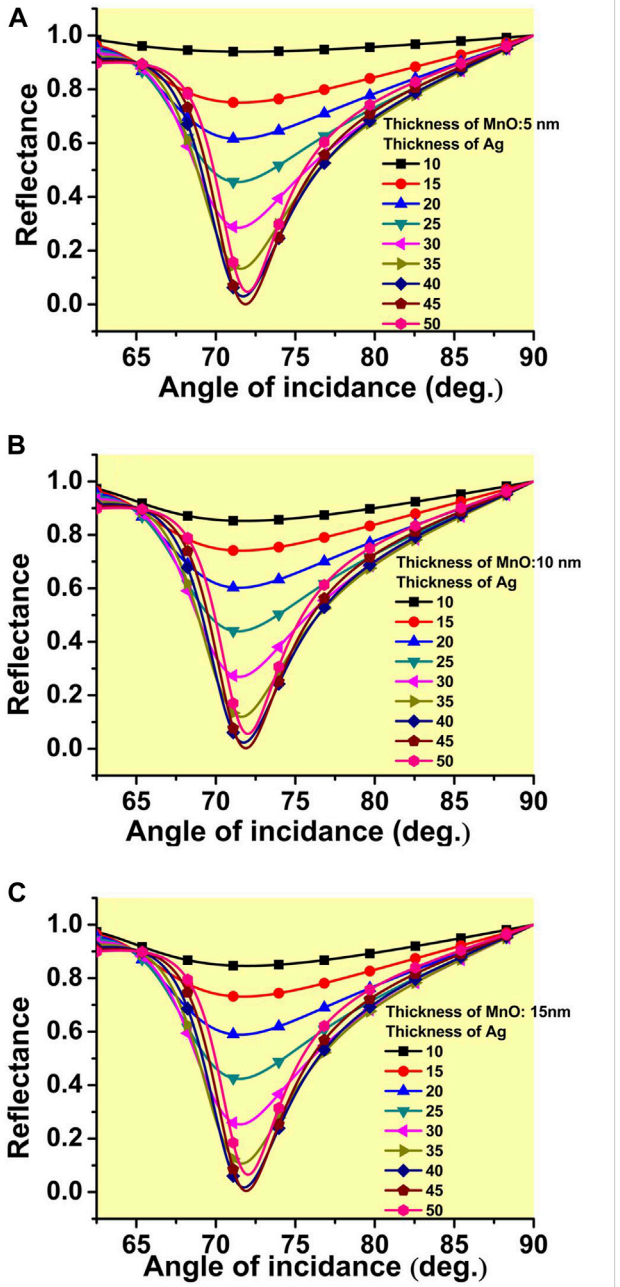

FIGURE 2
The optimization of the thickness of the Ag metal placed on the adhesion layer of MgO having a thickness. **(A)** 5 nm, **(B)** 10 nm, and **(C)** 15 nm.

3 Mathematical modeling

3.1 Mathematical modeling for reflectivity calculation

The paramount prerequisite for investigating the performance of the SPR sensor is to calculate the reflectivity (reflectance or reflection intensity) of the incident light at the output terminal. The transfer matrix method (TMM) is the most efficient way since there is no need to apply any approximation for measuring the reflectivity of the incident light at the output. The reflectivity of incident light is calculated from the light bounced back through the interface of the metal dielectric of the N-layer model (Wang et al., 2012). This methodology provides the most accurate outcomes when a customized MATLAB program is developed to compute the harmony of SPR modulation. Hence, Matlab software is used to calculate the SPR modulation for the N-layer model. All the layers are stacked in the vertical direction (z-axis) of the BK7 glass-coupling prism. In the layered structure SPR, a correlation between the tangential component of the propagating SPW with the initial and final limit, i.e., $Z = Z_1 = 0$ and $Z = Z_{N-1}$. This correlation between the initial and final limit is written in Eq. 3, as per the report in (Rahman et al., 2017).

$$\begin{bmatrix} U_1 \\ V_1 \end{bmatrix} = M \begin{bmatrix} U_{N-1} \\ V_{N-1} \end{bmatrix} \tag{3}$$

Here, U_1 and V_1 are representing the components of the electric and magnetic field respectively along the tangential direction at the boundary of the first layer while, U_{N-1} and V_{N-1} are representing the corresponding fields for the boundary at the nth layer. Now, a characteristic architecture of the composite structure is represented by M_{ij} as given in Eq. 4.

$$M_{ij} = \left(\prod_{k=2}^{n-1} M_k \right) = \begin{bmatrix} M_{11} & M_{12} \\ M_{21} & M_{22} \end{bmatrix} \tag{4}$$

where,

$$M_k = \begin{bmatrix} \mathrm{Cos}\,\alpha_k & (-i * \mathrm{Sin}\,\alpha_k)/q_k \\ -iq_k \mathrm{Sin}\,\alpha_k & \mathrm{Cos}\,\alpha_k \end{bmatrix} \tag{6}$$

Here, α_k is representing an arbitrary phase constant for the kth layer and q_k is defined in the

$$\alpha_k = (2\pi/\lambda) n_k \mathrm{Cos}\,\theta_k (z_k - z_{k-1}) = \left(\frac{2\pi d_k}{\lambda} \right) (\varepsilon_k - n_1^2 \mathrm{Sin}^2 \theta_1)^{1/2}$$

and,

$$q_k = \left(\frac{\mu_k}{\varepsilon_k} \right)^{\frac{1}{2}} \mathrm{Cos}\,\theta_{k=} (\varepsilon_k - n_1^2 \mathrm{Sin}^2 \theta_1)^{\frac{1}{2}} / \varepsilon_k$$

Where, θ and λ are representing the angle of incidence and the wavelength of the incident light. Also, n is denoting the refractive index of the prism while ε_k is the dielectric constant for the kth layer.

Finally, on solving the above equation, the reflection coefficient/reflectance for the incident light beam is given in Eq. 7 as reported in (Rahman et al., 2017).

$$r = \frac{(M_{11} + M_{12} q_n) q_1 - (M_{21} + M_{22} q_n)}{(M_{11} + M_{12} q_n) q_1 + (M_{21} + M_{22} q_n)} \tag{7}$$

At last, the reflection intensity for plane-polarized light is calculated by Eq. 8, as reported in (Zeng et al., 2015).

$$R = |r|^2 \tag{8}$$

The resonance angle (θ_{SPR}) for the SPR sensor is based on the shifts in the resonance angle, which depends upon the effective RI of the layered material involved and the RI of the sensing medium or analyte (Dey et al., 2021). In SPR sensors, a minute change in the RI of the sensing medium can be detected by the shift in the resonance

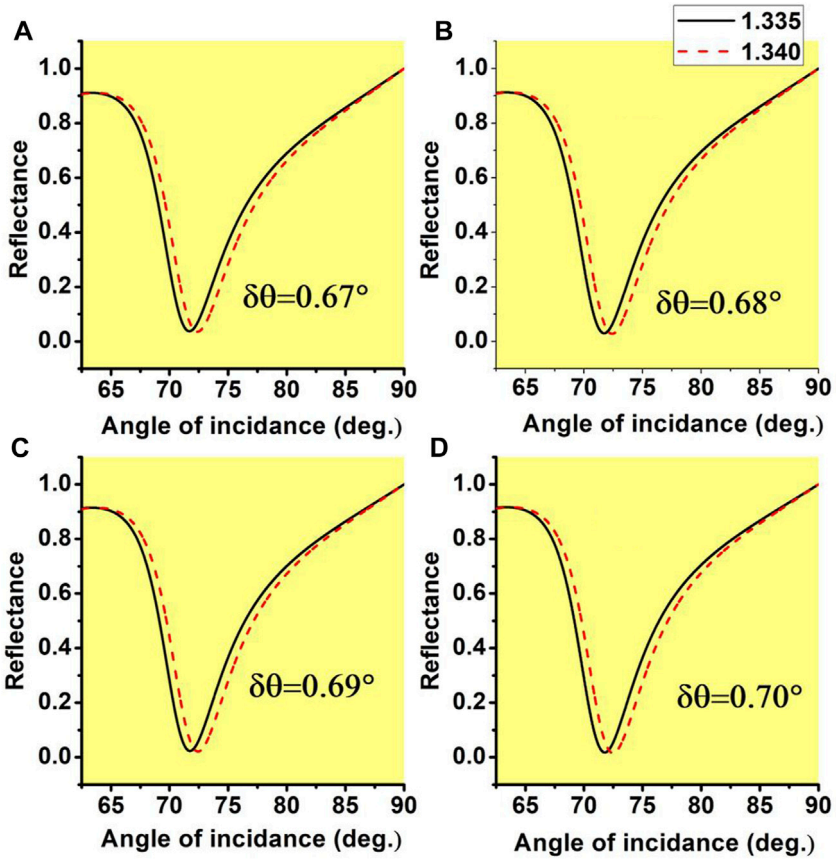

FIGURE 3
The variation of the reflectance with the angle of the incidence of the prism for the two RI of the analyte 1.335 and 1.340 when the thickness of the adhesion layer of MgO is considered as **(A)** 0 nm **(B)** 5 nm **(C)** 10 nm **(D)** 15 nm.

angle θ_{SPR} and the shift of the resonance angle is measured by the Eq. 9 as in (Dey et al., 2021).

$$\theta_{SPR} = \sin^{-1}\frac{n_{effective} * n_{analyte}}{n_{prism}\left(n^2_{effective} + n^2_{analyte}\right)^{1/2}} \quad (9)$$

Here, $n_{effective}$ represents the refractive index of the composite layer.

3.2 Performance evaluating parameters of SPR sensor

The performance characteristic of the SPR sensor significantly depends on the resonance angle, i.e., the angle that depicts the change in the RI of the sensing medium or analyte. The resonance angle of the SPR can be defined as the angle where minimum reflectance is detected, corresponding to the incident angle of the light. Three main parameters define the quality of the SPR sensors. The parameters are the sensitivity of the sensor (S), detection accuracy (DA), and quality factor (QF). The parameter, as mentioned above, should be as high as possible for better performance of the SPR sensors. However, another parameter that has a significant impact on the above-mentioned SPR sensor characteristics is the full-width-half maximum (FWHM). The FWHM quantity should be as small as possible compared to the characteristic parameters. Sensitivity (S) is the most critical parameter, which is defined as the ratio between the resonance angle change ($\delta\theta$) with RI variation (δn) in the analyte or sensor medium. The dimension is measured in terms of the refractive index unit (termed as RIU^{-1}) and is calculated through Eq. 10 as in (Rahman et al., 2017; Dey et al., 2021).

$$S = \frac{\delta\theta}{\delta n} \quad (10)$$

Detection Accuracy (DA) is defined as the inverse of the FWHM. The FWHM can be calculated through the thickness of the SPR curve at half (50%) of reflectivity. The dimension of DA is 1/deg and is calculated by the Eq. 11 as in (Rahman et al., 2017; Dey et al., 2021).

$$DA = \frac{1}{FWHM} \quad (11)$$

Another important parameter for getting clear concept of the sensing efficiency is the measurement of figure of merit (FOM). It is also known as the quality factor (QF) of the sensor. Its dimension is in RIU^{-1} and can be defined by the Eq. 12 as in (Rahman et al., 2017; Dey et al., 2021).

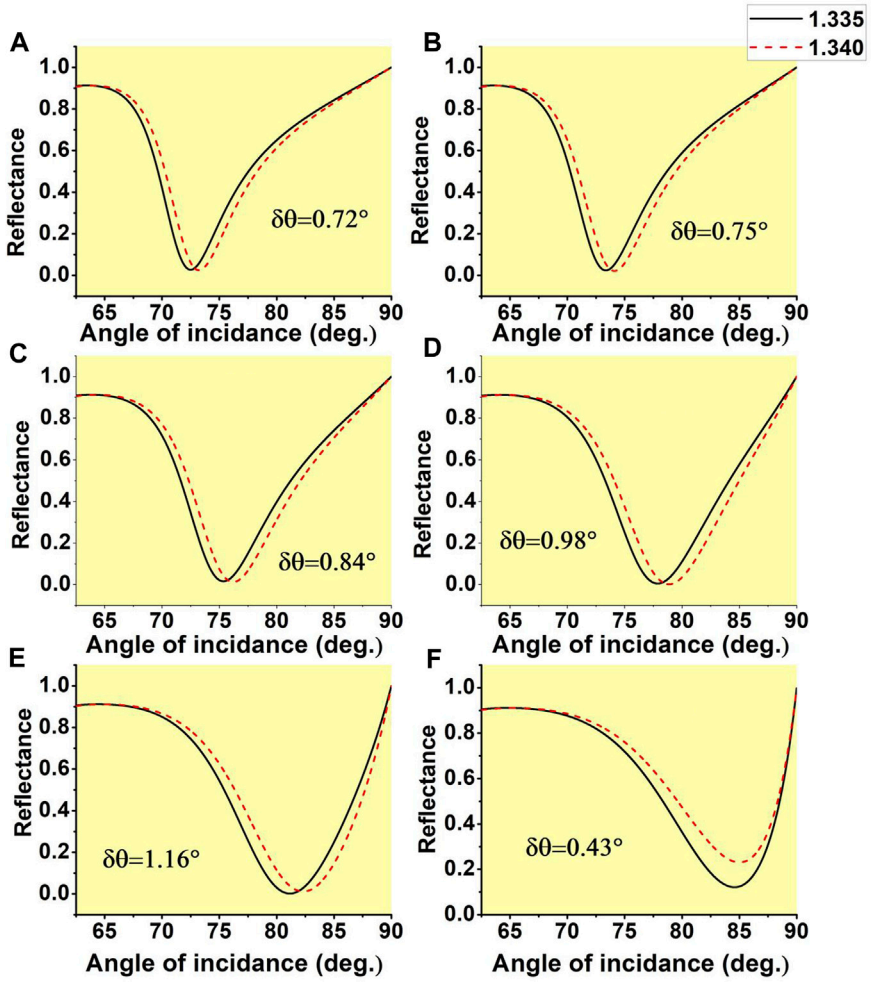

FIGURE 4
The variation of the reflectance with the angle of the incidence of the prism for the two RI of the analyte 1.335 and 1.340 when the thickness of the adhesion layer of MgO is considered as 5 nm, while the number of BP layers on Ag are **(A)** 1 layer **(B)** 2 layers **(C)** 4 layers **(D)** 6 layers **(E)** 8 layers **(F)** 10 layers.

$$FOM = \frac{S}{FWHM} \tag{12}$$

4 Results and discussion

The main target of the proposed structure is to improve the performance and sensitivity as high as possible. As discussed in the previous section, this requirement can be fulfilled by selecting a low refractive index prism for the coupling of incident light. Therefore, the BK7 prism is chosen for the light coupling since its refractive index value is lower. However, in contrast to the low refractive index prism, a high refractive index prism will provide a sharp dip in the resonance curve. Indeed, there are several other advantages of using a low-RI prism that shadows the benefits of a high-RI prism. A low-RI prism provides better SPR resonance FWHM, the shift in the resonance curve, and the resonance angle; as a result, it becomes possible to receive high sensitivity.

As discussed in Section 2, the proposed SPR sensor consists of five layers. At first, an adhesion layer of MgO is deposited on top of the BK7 prism. The third layer is a silver metal layer on top of the MgO. The adhesion layer of MgO ensures firm bonding between the metal (Ag) and the substrate layers (prism). To begin with the analysis, three thicknesses of the adhesion layer (MgO) are chosen for the optimization of the Ag. The thickness of MgO are considered to be 5 nm, 10 nm, and 15 nm, and thickness optimization of the Ag material is performed in each case. Figure 2A shows the optimization of the Ag metal, which is placed on the 5 nm thick MgO. The reflectance is measured using the TMM method, as discussed in the previous section. Further, the reflectance is recorded for varying thicknesses of the Ag material, considering the RI of the analyte is 1.335 in each case.

The figure shows that the increment in thickness delivers better reflectance, reflecting the excellent increment in the absorption of the incident light. It can be observed that the rate of decrement in reflectance slows down as the thickness increases beyond 35 nm. It is almost saturating at the 40 nm thick Ag metal layer. However, on a very careful observation, a further decrement in reflectance from a 40 nm to a 45 nm thick Ag metal layer is also recorded. Thereafter, a significant increment in reflectance is observed. For the case of

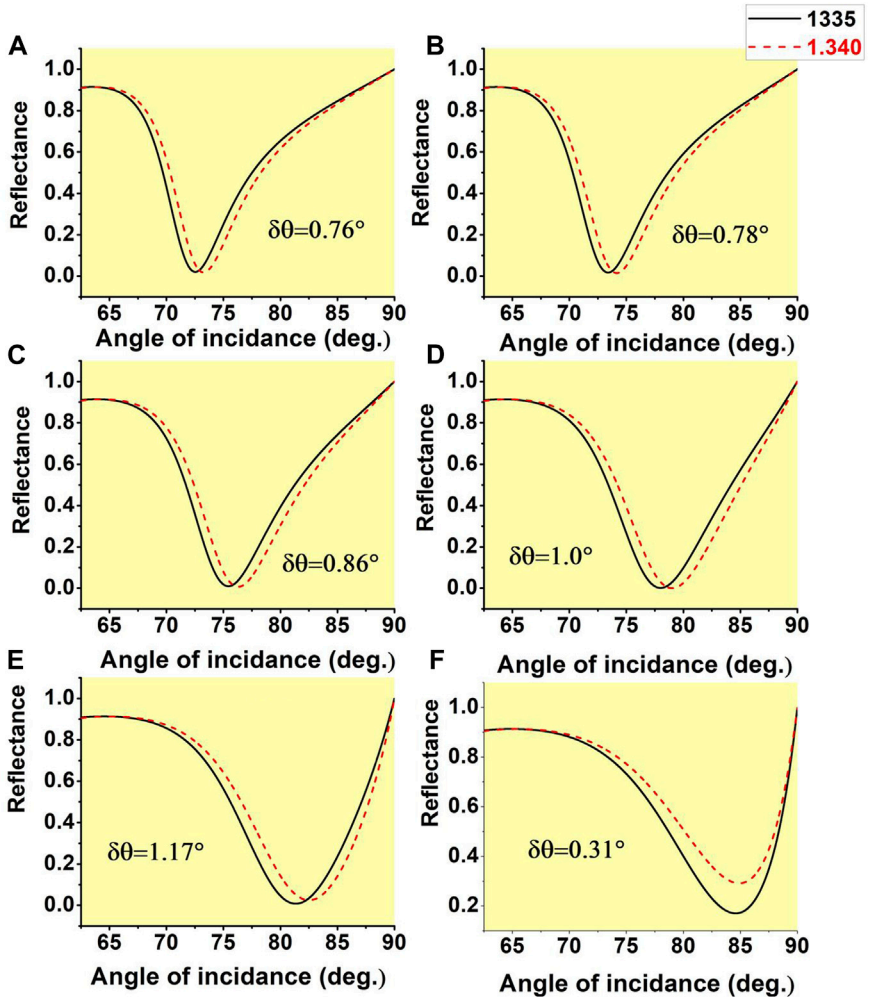

FIGURE 5
The variation of the reflectance with the angle of the incidence of the prism for the two RI of the analyte 1.335 and 1.340 when the thickness of the adhesion layer of MgO is considered as 10 nm, while the number of BP layers on Ag are **(A)** 1 layer **(B)** 2 layers **(C)** 4 layers **(D)** 6 layers **(E)** 8 layers **(F)** 10 layers.

10 nm and 15 nm thick MgO, a similar phenomenon or even a closer reflectance is recorded for the case of 40 nm and 45 nm thick Ag metal layers, as can be seen from Figures 2B, C, respectively. However, in the case of 15 nm, the curve of 40 nm and 45 nm thick Ag is almost overlapping. Hence, considering the aforementioned phenomenon of a minute increment of the reflectance between the 40 nm and 45 nm metal layers of Ag, so 40 nm thickness of the Ag is considered for further optimization. The thinner layer reduces the cost of the device and may be suitable for enhancing the SPR phenomenon. The final optimized reflectance at 40 nm thick Ag metal for cases of 5 nm, 10 nm, and 15 nm thick MgO are found to be 0.029, 0.023, and 0.017, respectively. Now, before going forward, it will be relevant to calculate the sensitivity at this configuration stage. The refractive index of the analyte or biosample is considered to vary from 1.335 to 1.340. For ease of calculation, the deviation in the resonance angle is calculated cross-ponding to the RI as mentioned above only, i.e., 1.335 and 1.340. More explicitly, sensitivity is measured by the deviation in the refractive index of 0.005 from 1.335.

Figure 3 depicts reflectance as a function of the incident light angle at the stage of Ag metal with the analyte kept on it. The reflectance is calculated when the thickness of the MgO varies from 0 nm to 15 nm. The solid black curve shows reflectance for the analyte of RI 1.335, while the red dashed curve shows the same for RI 1.340. The analysis shows that as the thickness of the adhesion layer MgO increases, a slight improvement in the deflection angle, as well as the minimum reflectance, is recorded. It reflects a slight improvement in the absorption of the incident light. At this stage, the sensitivities range from 134°RIU^{-1} to 140°RIU^{-1} (Refractive Index Unit-RIU). Here, it should be noted that the deflection angle indicates the difference in the angle recorded between the RI of the analyte of 1.335 and 1.340, corresponding to their lowest reflectance considered for the analysis of the SPR sensor, and corresponding to the 5 nm, 10 nm, and 15 nm thickness of the adhesive layer of MgO, respectively. As discussed in the previous section, using 2D materials (BP) has several advantages in SPR. Therefore, further analysis is carried out by placing some layers of BP on the 40 nm thick Ag metal layer. A systematic analysis is

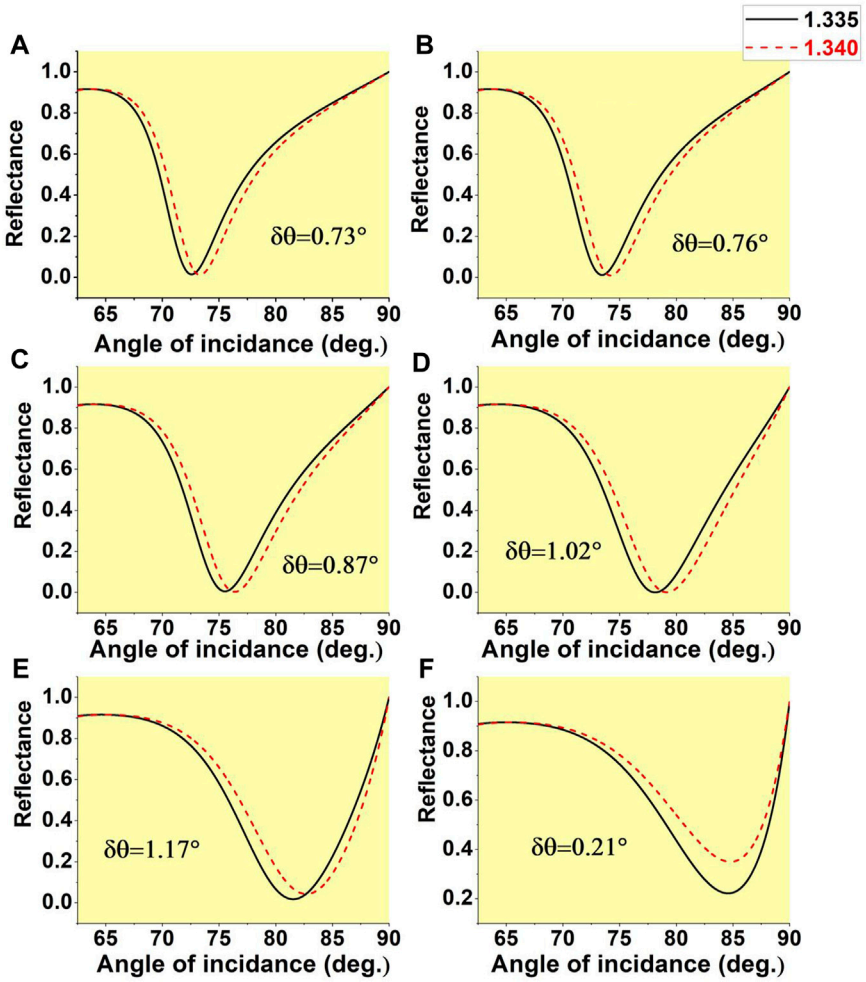

FIGURE 6
The variation of the reflectance with the angle of the incidence of the prism for the two RI of the analyte 1.335 and 1.340 when the thickness of the adhesion layer of MgO is considered as 15 nm, while the number of BP layers on Ag are **(A)** 1 layer **(B)** 2 layers **(C)** 4 layers **(D)** 6 layers **(E)** 8 layers **(F)** 10 layers.

TABLE 2 Sensitivity outcomes layer by layer with several configuration.

Layers	Configuration with thickness	Sensitivity (°RIU^{-1})
1	BK7	----
2	BK7/Ag (40 nm)/Analyate	134
3	BK7/MgO (5 nm)/Ag (40 nm)/Analyate	136
	BK7/MgO (10 nm)/Ag (40 nm)/Analyate	138
	BK7/MgO (15 nm)/Ag (40 nm)/Analyate	140
4	BK7/MgO (5 nm)/Ag (40 nm)/BP (8 layers)/Analyate	232
	BK7/MgO (10 nm)/Ag (40 nm)/BP (8 layers)/Analyate	234
	BK7/MgO (15 nm)/Ag (40 nm)/BP (8 layers)/Analyate	234

performed by increasing the number of BP layers on Ag. Here, three cases are possible. In the first case, a 40 nm thickness of the Ag metal on the 5 nm thick adhesion layer of MgO is considered for the analysis. The performance of the SPR sensor is calculated by increasing the number of layers of BP on the metal. Figure 4 shows the reflectance variation as a function of incident angle

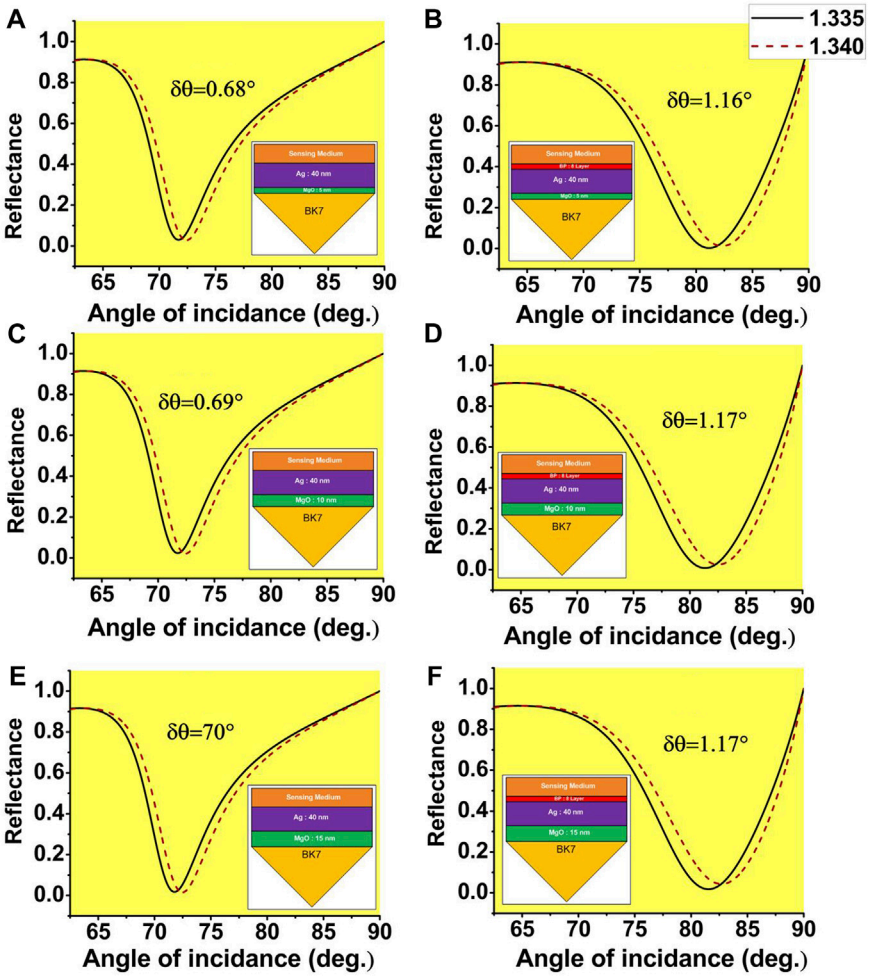

FIGURE 7
Variation of the reflectance with the angle of the incidence of the prism for two RI of the analyte 1.335 and 1.340. When the thickness of the adhesion layer of MgO and BP are considered as **(A)** MgO = 5 nm, BP = 0, **(B)** MgO = 5 nm, BP = 8 layers, **(C)** MgO = 10 nm, BP = 0, **(D)** MgO = 10 nm, BP = 8 layers, **(E)** MgO = 15 nm, BP = 0, **(F)** MgO = 15 nm, BP = 8 layers.

TABLE 3 Comparison of the sensitivity and FOM with some of recently reported SPR sensors.

Ref.	Year	Configuration	Sensitivity	FOM
Meshginqalam and Barvestani (2018)	2018	SF6/Chromium/Au/BP/WS_2	187	---
Xu et al. (2019)	2019	BK7/Au/WS2/Au/MXene	198	--
Jia et al. (2019)	2020	BK7/Ag/$PtSe_2$	162	14.93
Jia et al. (2019)	2020	BK7/Au/$PtSe_2$	165	14.12
Nurrohman and Chiu (2021)	2020	BK7/Au/WSe_2/Graphene	178.8	27.86
Lin et al. (2020)	2020	SF11/Au/MoS_2/WS_2/WSe_2	142	--
Hossain et al. (2020)	2020	SF11/Au/MoS_2/Graphene	130	17.02
Kumar et al. (2020)	2020	BK7/ZnO/Ag/$BaTiO_3$/WS_2	180	---
Rikta et al. (2021)	2021	SF10/Au/α-$SnSe_2$/Phosphorene	96.4	12.36
Rahman et al. (2021)	2021	BK7/Au/WSe_2/$PtSe_2$/BP	200	17.70
	This work	BK7/MgO/Ag/BP	234	38.18

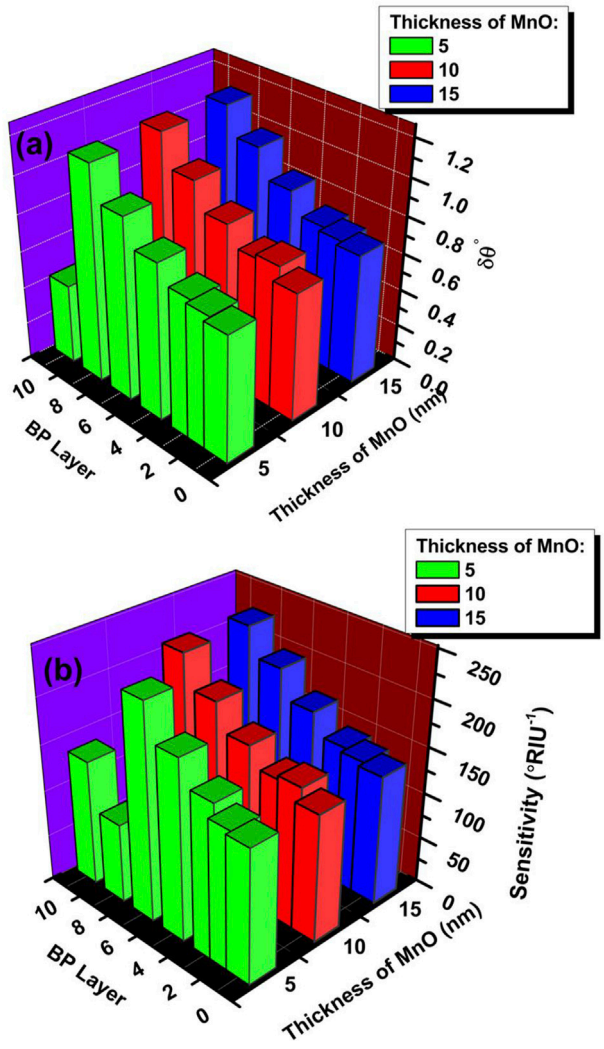

FIGURE 8
The variation of **(A)** deflection angle ($\delta\theta$), **(B)** Sensitivity with the number of layers of BP for the three thicknesses 5 nm, 10 nm, and 15 nm of MgO.

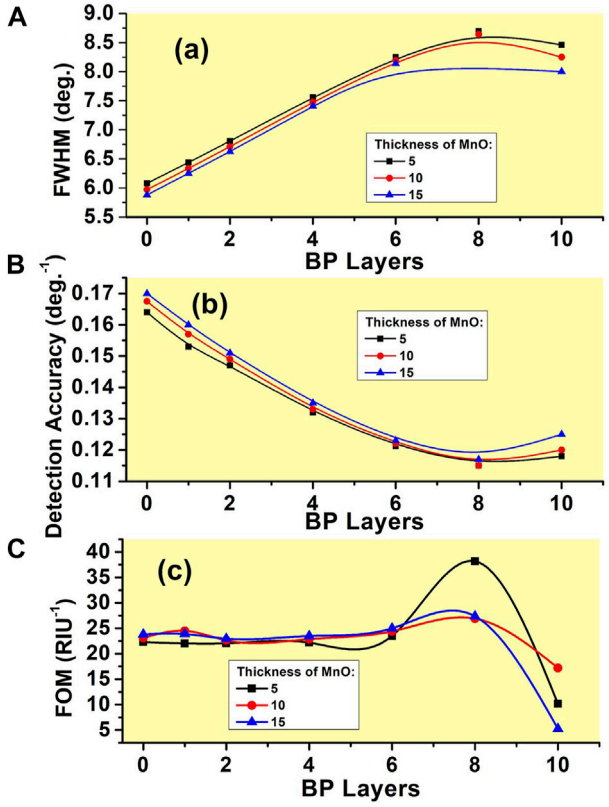

FIGURE 9
Variation of **(A)** FWHM **(B)** Detection accuracy (DA) **(C)** The figure of merit (FOM) with the increment of the number of layers of BP.

when the number of layers of BP increases from 1 layer to 10 layers. In Figure 4, the deflection angle increases from 0.72° to 1.16° for adding one layer to 8 layers of BP. It reflects the increment in the absorption of incident light in the analyte due to the large real part of the dielectric constant of the BP. Further increment of the BP, i.e., beyond eight layers, a significant deviation is observed; consequently, a decrease in the deflection angle is recorded.

It reflects that saturation is achieved on the eighth layer of the BP. The significant deflection in the resonance angle by placing layers of BP crossponds to a substantial improvement in the sensitivity of the proposed SPR sensors. The sensitivity improves from 134°RIU^{-1} to 232°RIU^{-1}. A similar analysis is performed considering the 10 nm and 15 nm thickness of the adhesive layer of MgO to calculate the impact on the performance of the proposed SPR-based sensors. Figure 5 shows the variation of reflectance as a function of incident angle for increasing the number of layers of BP, considering the 10 nm thickness of the MgO. It can be observed from Figure 5 a better deflection of the resonance angle is recorded as compared to the case of 5 nm thick MgO. In this case, also, saturation is achieved on the eighth layer of BP. However, the deflection angle is slightly large compared to the earlier one. As a result, an improved sensitivity performance is calculated as compared to the earlier one. Considering the fact of improvement in performance from the 5 nm–10 nm thick MgO layer, it will be relevant to check the performance for the thicker value of MgO. Hence, a further calculation is performed on a 15 nm thick MgO layer.

A similar analysis is performed to check the performance of the sensor. Figure 6 shows a similar reflectance curve for the case of 15 nm thick MgO. In this case, a more rapid deflection is observed, but the maximum deflection remains constant at the eighth layer as in the 10 nm thick MgO case. Therefore, it is concluded that the optimum performance can be achieved when 10 nm thick MgO is taken into consideration. Now, a summary of all three cases of MgO with and without the optimized eight layer of BP is presented in Figure 7. In Figure 7, the left-sided figures, i.e., (a), (c), and (e) are, showing reflectance with incident angles for 5 nm, 10 nm and 15 nm thick MgO respectively without considering BP layers. The right-side figure shows reflectance as a function of incident angle with eight layers of BP. It is concluded from this analysis 10 nm thick layer of MgO with eight layers of BP provides the optimum sensitivity performance of the proposed sensors.

Now, Figure 8 represents the deflection angle and sensitivity variation by varying the number of layers of BP for all three cases of the adhesion layer thickness of 5 nm, 10 nm, and 15 nm. It is clearly shown that maximum deflection and hence maximum sensitivity can be achieved by considering 10 nm MgO with eight layers of BP. Finally, the other important SPR sensor performing parameters, such as Detection Accuracy (DA), Figure of Merit (FOM), need to be calculated. As discussed in the previous section, this parameter depends on the full-width half maximum (FWHM) of the SPR. To get a high value of DA and FOM, the value of FWHM should be as low as possible, as FWHM is inversely proportional to the performing parameters. However, as the number of the BP layers is increasing, the value of FWHM is also increasing; consequently, DA is decaying. On the other hand, FOM is improving even though FWHM is increasing as can be seen in Figure 9. The maximum value of FOM is about 38.2°RIU^{-1} is calculated when a 5 nm thick MgO and eight layers of BP are taken into consideration. Moreover, the maximum value of DA of about 0.17 $deg.^{-1}$ is found for 15 nm thick MgO as FWHM is experiencing the lowest value.

Hence, it will be relevant here to summaries all sensitivity in the tabular form a quick review. Table 2 represents the layer-by-layer outcomes of the result. The Table represents the summary of all the sensitivity of several configuration along with their thickness.

Finally, a comparison Table 3 has been prepared to compare the proposed novel structure of SPR sensor performance with some earlier proposed SPR sensors performance. Thereafter a conclusion is presented that summarizes the complete work.

5 Conclusion

In this work, a Kretschmann configuration based on a hybrid structure is proposed to improve the performance of the surface plasmon resonance (SPR) sensor working on the visible light region. The structure is based on five layers, in which first and fifth layers are the BK7 prism and analyte/sensing medium. On top of the prism, an adhesion layer made of magnesium oxide (MgO) is incorporated to avoid the adverse effect, which causes a broadening and decrease in the resonance magnitude. The third layer is a silver metal layer thereafter few layers of black phosphorus (BP), a 2D material, are added. The performance of the sensor is analyzed by calculating the reflectance for two fixed refractive indices, 1.335 and 1.340, of the analyte using the transfer matrix method (TMM). A complete investigation is carried out considering various thicknesses of the MgO and layers of the BP to get optimized maximum performance of the sensor. The maximum sensitivity is found to be 234°RIU^{-1} for 10 nm thickness MgO, 40 nm Ag and eight layers of BP. Additionally, the maximum figure of merit (FOM) and detection accuracy are recorded as 38.18°RIU^{-1} and 0.17 $deg.^{-1}$, respectively. With such an excellent performance and simple structure, the sensor may be expected to be used in several petitions of biological and biochemical sensing applications.

Data availability statement

The original contributions presented in the study are included in the article/Supplementary Material, further inquiries can be directed to the corresponding author.

Author contributions

All authors listed have made a substantial, direct, and intellectual contribution to the work and approved it for publication.

Conflict of interest

The authors declare that the research was conducted in the absence of any commercial or financial relationships that could be construed as a potential conflict of interest.

Publisher's note

All claims expressed in this article are solely those of the authors and do not necessarily represent those of their affiliated organizations, or those of the publisher, the editors and the reviewers. Any product that may be evaluated in this article, or claim that may be made by its manufacturer, is not guaranteed or endorsed by the publisher.

References

Abbott, W. M., Murray, C. P., Zhong, C., Smith, C., McGuinness, C., Rezvani, E., et al. (2019). Less is more: Improved thermal stability and plasmonic response in Au films via the use of subnanometer Ti adhesion layers. *ACS Appl. Mater. Interfaces* 11 (7), 7607–7614. doi:10.1021/acsami.8b21193

Akowuah, E. K., Gorman, T., and Haxha, S. (2009). Design and optimization of a novel surface plasmon resonance biosensor based on Otto configuration. *Opt. Express* 17 (26), 23511–23521. doi:10.1364/oe.17.023511

Aouani, H., Wenger, J., Gérard, D., Rigneault, H., Devaux, E., Ebbesen, T. W., et al. (2009). Crucial role of the adhesion layer on the plasmonic fluorescence enhancement. *ACS Nano* 3 (7), 2043–2048. doi:10.1021/nn900460t

Asif, M., Ajmal, M., Ashraf, G., Muhammad, N., Aziz, A., Iftikhar, T., et al. (2020). The role of biosensors in coronavirus disease-2019 outbreak. *Curr. Opin. Electrochem.* 23, 174–184. doi:10.1016/j.coelec.2020.08.011

Bellassai, N., D'Agata, R., Jungbluth, V., and Spoto, G. (2019). Surface plasmon resonance for biomarker detection: advances in non-invasive cancer diagnosis. *Front. Chem.* 7, 570. doi:10.3389/fchem.2019.00570

Bruna, M., and Borini, S. J. A. P. L. (2009). Optical constants of graphene layers in the visible range. *Appl. Phys. Lett.* 94 (3), 031901. doi:10.1063/1.3073717

Castellanos-Gomez, A. (2015). Black phosphorus: narrow gap, wide applications. *J. Phys. Chem. Lett.* 6 (21), 4280–4291. doi:10.1021/acs.jpclett.5b01686

Cho, S. Y., Lee, Y., Koh, H. J., Jung, H., Kim, J. S., Yoo, H. W., et al. (2016). Superior chemical sensing performance of black phosphorus: comparison with MoS2 and graphene. *Adv. Mater.* 28 (32), 7020–7028. doi:10.1002/adma.201601167

Dey, B., Islam, M. S., and Park, J. (2021). Numerical design of high-performance WS2/metal/WS2/graphene heterostructure based surface plasmon resonance refractive index sensor. *Results Phys.* 23, 104021. doi:10.1016/j.rinp.2021.104021

Djaker, N., Hostein, R., Devaux, E., Ebbesen, T. W., Rigneault, H., and Wenger, J. (2010). Surface enhanced Raman scattering on a single nanometric aperture. *J. Phys. Chem. C* 114 (39), 16250–16256. doi:10.1021/jp104971p

Ekgasit, S., Thammacharoen, C., Yu, F., and Knoll, W. (2005). Influence of the metal film thickness on the sensitivity of surface plasmon resonance biosensors. *Appl. Spectrosc.* 59 (5), 661–667. doi:10.1366/0003702053945994

Gupta, B. D., and Sharma, A. K. (2005). Sensitivity evaluation of a multi-layered surface plasmon resonance-based fiber optic sensor: a theoretical study. *Sens. Actuators B Chem.* 107 (1), 40–46. doi:10.1016/j.snb.2004.08.030

Hossain, M. B., Kabir, M. A., Hossain, M. S., Islam, K. Z., Hossain, M. S., Pathan, M. I., et al. (2020). Numerical modeling of MoS2–graphene bilayer-based high-performance surface plasmon resonance sensor: structure optimization for DNA hybridization. *Opt. Eng.* 59 (10), 105105. doi:10.1117/1.oe.59.10.105105

Hughes, H., Bussmann, K., McMarr, P. J., Cheng, S. F., Shull, R., Chen, A. P., et al. (2012). Radiation studies of spin-transfer torque materials and devices. *IEEE Trans. Nucl. Sci.* 59 (6), 3027–3033. doi:10.1109/tns.2012.2223487

Jeppesen, C., Mortensen, N. A., and Kristensen, A. (2010). The effect of Ti and ITO adhesion layers on gold split-ring resonators. *Appl. Phys. Lett.* 97 (26), 263103. doi:10.1063/1.3532096

Jia, Y., Li, Z., Wang, H., Saeed, M., and Cai, H. (2019). Sensitivity enhancement of a surface plasmon resonance sensor with platinum diselenide. *Sensors* 20 (1), 131. doi:10.3390/s20010131

Khamh, H., Sachet, E., Kelly, K., Maria, J. P., and Franzen, S. (2018). As good as gold and better: conducting metal oxide materials for mid-infrared plasmonic applications. *J. Mater. Chem. C* 6 (31), 8326–8342. doi:10.1039/c7tc05760a

Kumar, A., Yadav, A. K., Kushwaha, A. S., and Srivastava, S. K. (2020). A comparative study among WS2, MoS2 and graphene based surface plasmon resonance (SPR) sensor. *Sens. Actuators Rep.* 2 (1), 100015. doi:10.1016/j.snr.2020.100015

Li, L., Liang, Y., Guang, J., Cui, W., Zhang, X., Masson, J. F., et al. (2017). Dual Kretschmann and Otto configuration fiber surface plasmon resonance biosensor. *Opt. express* 25 (22), 26950–26957. doi:10.1364/oe.25.026950

Lin, Z., Chen, S., and Lin, C. (2020). Sensitivity improvement of a surface plasmon resonance sensor based on two-dimensional materials hybrid structure in visible region: A theoretical study. *Sensors* 20 (9), 2445. doi:10.3390/s20092445

Mauriz, E. (2020). Recent progress in plasmonic biosensing schemes for virus detection. *Sensors* 20 (17), 4745. doi:10.3390/s20174745

Meshginqalam, B., and Barvestani, J. (2018). Performance enhancement of SPR biosensor based on phosphorene and transition metal dichalcogenides for sensing DNA hybridization. *IEEE sensors J.* 18 (18), 7537–7543. doi:10.1109/jsen.2018.2861829

Najiminaini, M., Vasefi, F., Kaminska, B., and Carson, J. J. (2011). Optical resonance transmission properties of nano-hole arrays in a gold film: effect of adhesion layer. *Opt. express* 19 (27), 26186–26197. doi:10.1364/oe.19.026186

Nguyen, H. H., Park, J., Kang, S., and Kim, M. (2015). Surface plasmon resonance: a versatile technique for biosensor applications. *Sensors* 15 (5), 10481–10510. doi:10.3390/s150510481

Nurrohman, D. T., and Chiu, N. F. (2021). A review of graphene-based surface plasmon resonance and surface-enhanced raman scattering biosensors: Current status and future prospects. *Nanomaterials* 11 (1), 216. doi:10.3390/nano11010216

Otte, M. A., Estévez, M. C., Carrascosa, L. G., González-Guerrero, A. B., Lechuga, L. M., and Sepúlveda, B. (2011). Improved biosensing capability with novel suspended nanodisks. *J. Phys. Chem. C* 115 (13), 5344–5351. doi:10.1021/jp110363a

Otto, A. (1968). Excitation of nonradiative surface plasma waves in silver by the method of frustrated total reflection. *Zeitschrift für Physik A Hadrons Nucl.* 216 (4), 398–410. doi:10.1007/bf01391532

Pandey, P. S., and Raghuwanshi, S. K. (2022). Sensitivity enhancement of surface plasmon resonance (SPR) sensor assisted by BlueP/MoS 2 based composite heterostructure. *IEEE Access* 10, 116152–116159. doi:10.1109/access.2022.3219439

Rahman, M. S., Anower, M. S., Hasan, M. R., Hossain, M. B., and Haque, M. I. (2017). Design and numerical analysis of highly sensitive Au-MoS2-graphene based hybrid surface plasmon resonance biosensor. *Opt. Commun.* 396, 36–43. doi:10.1016/j.optcom.2017.03.035

Rahman, M. M., Rana, M. M., Anower, M. S., Sakib, N., Chakrabatri, K., and Paul, A. K. (2020). "An SPR-based optical biosensor with shared plasmonic materials and optimized graphene layer: An angular interrogation approach," in 2020 IEEE Region 10 Symposium (TENSYMP) (IEEE), 1680–1683.

Rahman, M. M., Abdulrazak, L. F., Ahsan, M., Based, M. A., Rana, M. M., Anower, M. S., et al. (2021). 2D nanomaterial-based hybrid structured (Au-WSe 2-PtSe 2-BP) surface plasmon resonance (SPR) sensor with improved performance. *IEEE Access* 10, 689–698. doi:10.1109/access.2021.3137420

Rhodes, C., Franzen, S., Maria, J. P., Losego, M., Leonard, D. N., Laughlin, B., et al. (2006). Surface plasmon resonance in conducting metal oxides. *J. Appl. Phys.* 100 (5), 054905. doi:10.1063/1.2222070

Rhodes, C., Cerruti, M., Efremenko, A., Losego, M., Aspnes, D. E., Maria, J. P., et al. (2008). Dependence of plasmon polaritons on the thickness of indium tin oxide thin films. *J. Appl. Phys.* 103 (9), 093108. doi:10.1063/1.2908862

Rikta, K. A., Anower, M. S., Rahman, M. S., and Rahman, M. M. (2021). SPR biosensor using SnSe-phosphorene heterostructure. *Sens. Bio-Sensing Res.* 33, 100442. doi:10.1016/j.sbsr.2021.100442

Sadri-Moshkenani, P., Khan, M. W., Shafiqul Islam, M., Montoya, E., Krivorotov, I., Bagherzadeh, N., et al. (2020). Effect of magnesium oxide adhesion layer on resonance behavior of plasmonic nanostructures. *Appl. Phys. Lett.* 116 (24), 241601. doi:10.1063/5.0008665

Sahu, S. K., Reddy, S. K., Singh, M., and Avrutin, E. (2022). Hybrid plasmonic waveguide based platform for refractive index and temperature sensing. *IEEE Photonics Technol. Lett.* 34 (18), 953–956. doi:10.1109/lpt.2022.3195666

Sharma, A. K., Jha, R., and Pattanaik, H. S. (2010). Design considerations for surface plasmon resonance based detection of human blood group in near infrared. *J. Appl. Phys.* 107 (3), 034701. doi:10.1063/1.3298503

Stephens, R. E., and Malitson, I. H. (1952). Index of refraction of magnesium oxide. *J. Res. Natl. Bureau Stand.* 49 (4), 249–252. doi:10.6028/jres.049.025

Taha, B. A., Al Mashhadany, Y., Hafiz Mokhtar, M. H., Dzulkefly Bin Zan, M. S., and Arsad, N. (2020). An analysis review of detection coronavirus disease 2019 (COVID-19) based on biosensor application. *Sensors* 20 (23), 6764. doi:10.3390/s20236764

Verma, A., Prakash, A., and Tripathi, R. (2015). Sensitivity enhancement of surface plasmon resonance biosensor using graphene and air gap. *Opt. Commun.* 357, 106–112. doi:10.1016/j.optcom.2015.08.076

Wang, Q. H., Kalantar-Zadeh, K., Kis, A., Coleman, J. N., and Strano, M. S. (2012). Electronics and optoelectronics of two-dimensional transition metal dichalcogenides. *Nat. Nanotechnol.* 7 (11), 699–712. doi:10.1038/nnano.2012.193

Xu, Y., Ang, Y. S., Wu, L., and Ang, L. K. (2019). High sensitivity surface plasmon resonance sensor based on two-dimensional MXene and transition metal dichalcogenide: a theoretical study. *Nanomaterials* 9 (2), 165. doi:10.3390/nano9020165

Zeng, S., Yu, X., Law, W. C., Zhang, Y., Hu, R., Dinh, X. Q., et al. (2013). Size dependence of Au NP-enhanced surface plasmon resonance based on differential phase measurement. *Sens. Actuators B Chem.* 176, 1128–1133. doi:10.1016/j.snb.2012.09.073

Zeng, S., Hu, S., Xia, J., Anderson, T., Dinh, X. Q., Meng, X. M., et al. (2015). Graphene–MoS2 hybrid nanostructures enhanced surface plasmon resonance biosensors. *Sens. Actuators B Chem.* 207, 801–810. doi:10.1016/j.snb.2014.10.124